Current Optics and Photonics
Vol. 3, No. 5, October 2019, pp. 458-465

ISSN: 2508-7266(Print) / ISSN: 2508-7274(Online)
DOI: https://doi.org/10.3807/COPP.2019.3.5.458

Influences of Pump Spot Radius and Depth of Focus on the Thermal Effect of Tm:YAP Crystal

Hongliang Zhang, Ya Wen, Lin Zhang, Zhen Fan, Jinge Liu, and Chunting Wu*

College of Science, Changchun University of Technology, Changchun 130022, China

(Received May 16, 2019 : revised June 4, 2019 : accepted June 5, 2019)

The thermal effect and the light output of a laser crystal under different pumping depths were reported., Based on the thermal model of a single-ended pumped Tm:YAP crystal, the thermal stress coupled model used Comsol to theoretically calculate the effect of changing the pump spot size and pump depth on crystal heat distribution and stress distribution. The experimental results showed that the laser output power first increased and then decreased with increasing pump spot size. As the depth of focus increased, the laser output power first increased and then decreased. The experimental results were consistent with the theoretical simulation results. The theory of pump spot radius and depth of focus in this paper provided an effective simulation method for mitigating thermal effects, and provided theoretical supports for laser crystals to obtain higher laser output power.

Keywords : Tm:YAP crystal, Thermal effect, Depth of focus, Pump spot
OCIS codes : (140.3480) Lasers, diode-pumped; (140.6810) Thermal effects; (140.3580) Lasers, solid-state

I. INTRODUCTION

The 1.9 μm laser has wide application value in the fields of atmospheric environment gas monitoring, lidar, medical diagnosis and treatment, material processing and photoelectric countermeasures, for the reason that it is located in the weak absorption band of the atmosphere and is particularly safe for human eyes. In addition, 1.9 μm Tm:YAP laser is not only an excellent pumping source for a 2 μm Ho laser but also an efficient seed source of 8~12 μm mid-infrared OPO [10]. That was why the demand for high-power 1.9 μm lasers is becoming more and more prominent.

The thermal effect of the crystal seriously limits the output performance of the laser. It not only directly affects the pump speed, but also causes temperature quenching. Laser output power and beam quality cannot be improved. In addition, excessive crystal temperature can lead to internal thermal stress and crystal damage. The thermal effect of the laser crystal is one of the most important problems [1-3] which -affects the high power transmission of the solid laser. The end face of the crystal receives a large amount of pump energy when light pumps into the end face of the crystal. The temperature of the end face of the laser crystal rises, and the overall temperature distribution of the laser crystal is trapezoidal, which results in uneven temperature distribution [5]. Because of it, thermal stress is generated, causing thermal effects such as crystal deformation and thermal lens effect to affect the maximum pump power and conversion efficiency of the laser crystal. Finally it affects the output power and beam quality of the laser [9]. The thermal effect of the laser crystal is closely associated with the spot radius of the pump light and the depth of crystal focus, which not only affect the maximum pump power of the laser crystal, but also affect the laser gain.

In this paper, the heat distribution model was established by Comsol, which is finite element analysis software. By using the multi-physics coupling of solid heat transfer and solid mechanics modules, the internal temperature changing, the stress field of the end-pumped Tm:YAP crystal, the stress value at the maximum stress point and the overall

*Corresponding author: bigsnow1@163.com, ORCID 0000-0002-9765-4056
Color versions of one or more of the figures in this paper are available online.

deformation of the crystal under Gaussian pump light pumping were simulated, providing a theoretical basis for thermal lens effect analysis and crystal fragmentation limit. By simulating the temperature distribution of the crystal when changing the pump spot size and pump focus depth, the best focus spot and depth were obtained to achieve the maximum laser output. Through experimental verification of the theoretical analysis, at the focused spot was 300 μm, the depth of focus was 5 mm, the threshold power was 10.08 W, we got the maximum output power was 6.32 W. The research results provided a theoretical basis of the optimization of the high power laser.

II. Analysis of Thermal Field and Stress Field in Tm:YAP Crystal

As the end pump power increases, the temperature in the center of the laser crystal will be higher than the temperature at the edge, which will cause an uneven internal temperature and stress distribution, and the end surface will be deformed [4]. Finally, the thermal lens effect of the oscillating light in the laser crystal took place. A typical single-ended pump laser crystal structure is shown in Fig. 1.

The Tm:YAP laser crystal was wrapped in silver foil and placed in a copper water-cooled holder. It was cooled by a four-sided water-cooled cycle with a room temperature of 294 K and a water-cooler constant temperature of 289 K. The water cooling would remove some of the heat in the crystal, so a heat transfer process existed inside the crystal, and its thermal conductivity was constant k. Assuming that the pump light was approximated as a Gaussian distribution, the relationship between the light intensity distribution and the absorption coefficient and the spot radius can be obtained.

If the lateral distribution of the fiber-coupled LD output laser was an approximately Gaussian intensity distribution [6, 7]

$$I_p(r,z)=\frac{2P_p}{\pi\omega_p^2(z)}\exp(-\alpha z)\left(\frac{-2r^2}{\omega_p^2(z)}\right), \tag{1}$$

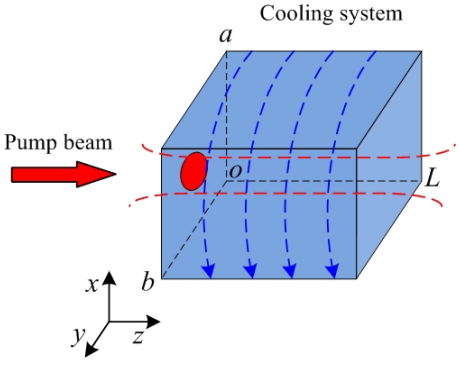

FIG. 1. Thermal model of Tm:YAP crystal for single-ended pump.

spot size ω_p was expressed as

$$\omega_p(r,z)=\omega_p^2\left(1+\left(\frac{(z-z_0)M_p^2\lambda_p}{n\pi\omega_p^2}\right)^2\right). \tag{2}$$

The heat source function $Q(r,z)$ can be expressed as

$$Q(r,z)=\frac{2P_p\alpha\xi}{\pi\omega_p^2(z)}\exp(-\alpha z)\exp\left(-\frac{2r^2}{\omega_p^2(z)}\right), \tag{3}$$

where P_p was the pump optical power and ξ was the thermal conversion coefficient. We converted it to Cartesian form as

$$Q(x,y,z)=\frac{2P_p\alpha\xi}{\pi\omega_p^2(z)}\exp(-\alpha z)\cdot\exp\left(-\frac{2(x^2+y^2)}{\omega_p^2(z)}\right). \tag{4}$$

The size of the Tm:YAP laser crystal was $3\times3\times15$ mm^3, corresponding to the x, y, and z directions, respectively. Pumping was from the end $z=0$ of the crystal, and the pump light direction was the same as the laser direction. The thermal conductivity was k when ignoring the anisotropy of the laser crystal. Its three-dimensional heat conduction equation was

$$\frac{\partial^2\Delta T}{\partial^2 x}+\frac{\partial^2\Delta T}{\partial^2 y}+\frac{\partial^2\Delta T}{\partial^2 z}=-\frac{1}{k}Q(x,y,z). \tag{5}$$

Keeping the heat sink temperature at T_b, and the air temperature at the end face T_0 by using water cooling at all four sides of the crystal ($y=\pm b/2$, $x=\pm a/2$), the boundary conditions considered were [8, 9]

$$\begin{aligned}
&k_x\frac{\partial T}{\partial x}|_{x=0}=h_s[T(0,y,z)-T_b],\\
&-k_x\frac{\partial T}{\partial x}|_{x=a}=h_s[T(a,y,z)-T_b],\\
&k_y\frac{\partial T}{\partial y}|_{y=0}=h_s[T(x,0,z)-T_b],\\
&-k_y\frac{\partial T}{\partial y}|_{y=b}=h_s[T(x,b,z)-T_b],\\
&k_z\frac{\partial T}{\partial z}|_{z=0}=h_a[T(x,y,0)-T_0],\\
&-k_z\frac{\partial T}{\partial z}|_{z=Lc}=h_a[T(x,y,Lc)-T_0],
\end{aligned} \tag{6}$$

where $k_x=k_y=7.2\,\mathrm{Wm^{-1}K^{-1}}$, $k_z=5.3\,\mathrm{Wm^{-1}K^{-1}}$, $h_s=1.5\times10^4\,\mathrm{Wm^{-1}K^{-1}}$, $h_a=5\,\mathrm{Wm^{-1}K^{-1}}$.

Next, the temperature stress model was mainly used to consider the model of stress, where x was the coefficient of thermal expansion. The above deformation cannot occur freely due to the external constraints in the elastic crystal and the mutual restraint between the various parts of the

body. Thus a stress change derived from temperature gradient was generated. The equilibrium equations coupled with the heat conduction equation can be obtained by using geometric equations, physical equations and equilibrium equations in elastic mechanics.

The equilibrium equation can be written as [10]

$$\begin{aligned}
&\frac{\partial \sigma_x}{\partial x}+\frac{\partial \sigma_{yx}}{\partial y}+\frac{\partial \sigma_{zx}}{\partial z}+K_x=0,\\
&\frac{\partial \sigma_y}{\partial y}+\frac{\partial \sigma_{zy}}{\partial z}+\frac{\partial \sigma_{xy}}{\partial x}+K_y=0,\\
&\frac{\partial \sigma_z}{\partial z}+\frac{\partial \sigma_{xz}}{\partial x}+\frac{\partial \sigma_{yz}}{\partial y}+K_z=0.
\end{aligned} \tag{7}$$

The geometric equation was

$$\begin{aligned}
&\varepsilon_x=\frac{\partial u}{\partial x} \quad \gamma_{xy}=\frac{\partial u}{\partial y}+\frac{\partial v}{\partial x},\\
&\varepsilon_y=\frac{\partial v}{\partial y} \quad \gamma_{yz}=\frac{\partial v}{\partial z}+\frac{\partial \omega}{\partial y},\\
&\varepsilon_z=\frac{\partial \omega}{\partial z} \quad \gamma_{zx}=\frac{\partial \omega}{\partial x}+\frac{\partial u}{\partial z}.
\end{aligned} \tag{8}$$

The equation of strain can be uniformly written as

$$\varepsilon_{ij'kl}+\varepsilon_{kl'ij}-\varepsilon_{ik'jl}-\varepsilon_{jl'ik}=0. \tag{9}$$

The physical equation can be written as

$$\varepsilon_{ij}=\frac{1+\mu}{E}\sigma_{ij}-\frac{\mu}{E}\delta_{ij}\sigma_{kk}+\alpha T, \tag{10}$$

$$\sigma_{ij}=2G\varepsilon_{ij}+\lambda\delta_{ij}\varepsilon_{kk}. \tag{11}$$

There was no displacement in the initial state, and the steady state was considered, so there was $u_i=0$ ($i=x, y, z$).

In Comsol 5.3, the static structural analysis in the "Structural Mechanics" interface was used to deal with thermal expansion, which was coupled by the solid heat transfer module-solid mechanics module. The parameters that used in the simulation were shown in TABLE 1. Considering the release action caused by crystal deformation due to thermal stress, the thermal stress coupling model described above was solved to obtain the temperature field and stress field distribution inside the crystal.

TABLE 1. Parameters of simulation

Parameter	Valve
Thermal conductivity k	11 W/m.K
Poisson's ratio v	0.3
dn/dT	10.08×10^{-6}/K
Thermal expansion coefficient α_T	9.6×10^{-6}/K
Absorption coefficient α	4.36/cm
Thermal conversion coefficient ξ	0.22
Crystal size	$3 \times 3 \times 15$ mm^3
Crystal refractive index	1.96
Spot radius ω_p	200~400 μm
Quality factor of pumping beam M^2_p	87

III. INFLUENCES OF DIFFERENT PUMP SPOT RADIUS AND DEPTH OF FOCUS ON HEAT DISTRIBUTION AND STRESS DISTRIBUTION IN THE CRYSTAL

3.1. Influence of Different Pump Spot Radius and Depth of Focus on Heat Distribution in the Crystal

One of the reasons for the thermal lens effect of the

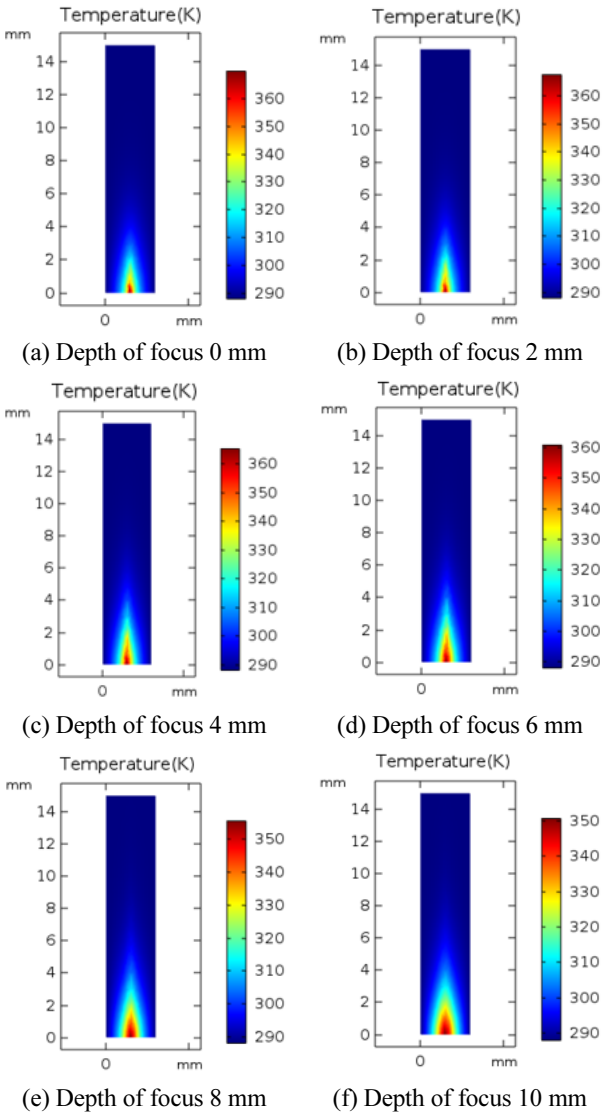

(a) Depth of focus 0 mm (b) Depth of focus 2 mm

(c) Depth of focus 4 mm (d) Depth of focus 6 mm

(e) Depth of focus 8 mm (f) Depth of focus 10 mm

FIG. 2. Internal temperature distributions in crystal at different depths of focus.

crystal was that the temperature distribution inside the crystal wasn't uniform and the temperature gradient was too sharp. Therefore, the temperature gradient would be reduced if the heat distribution of the pump light in the crystal was comparatively uniform, which would alleviate the thermal lens effect of the crystal. For this purpose, we considered changing the depth of focus of the pump light to avoid the waist of the pump light with highest optical density directly affecting the end face of the crystal. The temperature field distribution of the crystal was obtained by simulation. At this time, when the pumping power was 30 W, the pump spot radius was 300 μm, the temperature change in the crystal was simulated at the focal depths of 0 mm, 2 mm, 4 mm, 6 mm, 8 mm, and 10 mm, the results are shown in Fig. 2.

As shown in Fig. 2, as the depth of focus increased, the heated portion of the crystal also gradually increased. Specifically, in the Z-axis direction, the heated region became larger, the temperature gradient decreased, and the heat released portion was also spread. It is not only limited to the lower part of the crystal end face, but also is beneficial to the heat dissipation of the crystal and alleviation of the thermal lens effect caused by the temperature gradient.

It can be seen from Figs. 3 and 4 that when the depth of focus changed, the temperature field distribution in the crystal changed significantly. From the temperature distribution of the Y-axis at the end face of the crystal it was obviously visible that with the increased depth of focus, the maximum temperature in the crystal gradually decreased from 367.52 K to 350.62 K, which corresponds to a decrease of 16.9 K. When the part of the crystal along the Z-axis was gradually heated, the temperature distribution was extended. Although the depth of focus gradually increased, the maximum temperature distribution in the crystal was mainly concentrated in the end portion, because the pump light focused into the crystal and most of it was absorbed. The processes are shown in Fig. 5.

As shown in Fig. 5, whether the depth of focus was deep or shallow, it was required to pass through the end

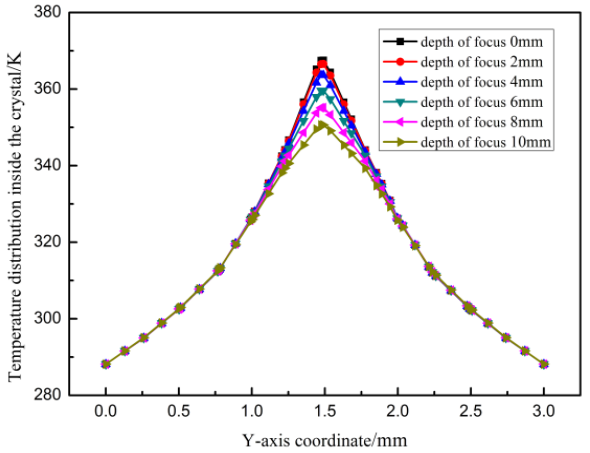

FIG. 3. Y-axis temperature distribution.

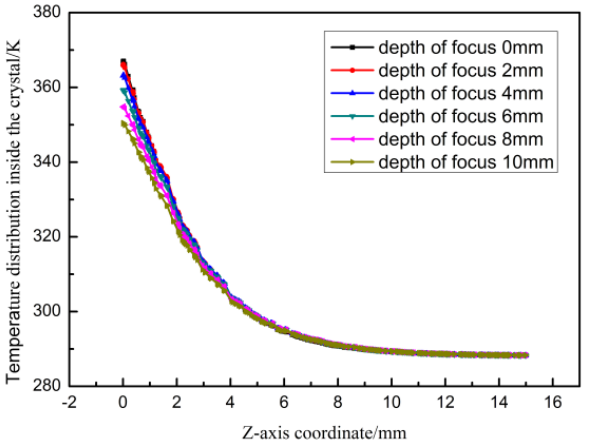

FIG. 4. Z-axis temperature distribution.

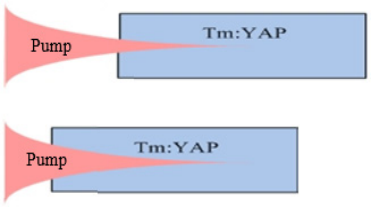

FIG. 5. Distributions of pump light in the crystal at different depths of focus.

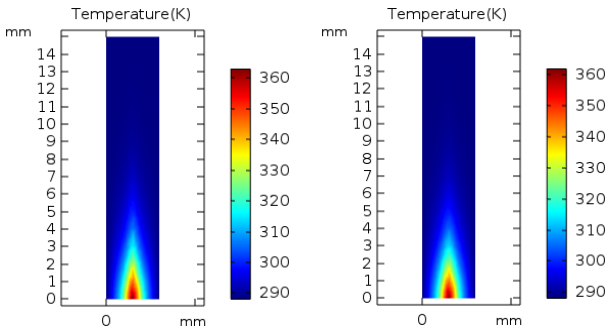

(a) Pump spot radius 200 μm (b) Pump spot radius 300 μm

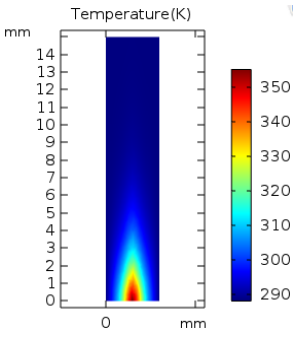

(c) Pump spot radius 400 μm

FIG. 6. Internal temperature distributions of the crystal at different pump spot radius.

face of the crystal. The temperature near the end face was still the highest, but the overall heating area was increased which was advantageous for heat conducting and relieved the thermal lens effect of the crystal. The spot radius of the pump light was changed by changing the coupling ratio of the focus coupling mirror, and the pump spot radii were 200 μm, 300 μm and 400 μm , the focus position was 5 mm, and the internal temperature distributions of the crystal are shown in Fig. 6.

It can be seen from Fig. 6 that as the focus coupling ratio increased, the internal temperature distribution region of the crystal and the area under pump power in the crystal both increased, thereby the internal maximum temperature of the crystal was reduced. The coupling ratios were 1 : 1, 1 : 1.5 and 1 : 2, the focus position was 5 mm, the maximum temperatures in the crystal were 362.83 K, 361.75 K, and 355.14 K, respectively.

Figure 7 shows variation of the maximum temperature at the end face of the crystal with the depth of focus changing when the pumping power was 30 W and the pump spot radius was 200 μm, 300 μm, and 400 μm. The maximum temperature in the crystal gradually decreased when the depth of focus increased. As the radius of the pump light spot increased, the maximum temperature in the crystal increased first and then decreased. Because of the increasing depth of focus, the pump light with a larger spot radius irradiated into the crystal, which resulted in a partial loss of energy. Therefore, the maximum temperature would be lower at the beginning, but as the depth of focus increased and the pump light diverged, the temperature inside the crystal gradually became stable. When the radius of the pump spot was small, the highest temperature in the crystal would decrease as the depth of focus increased. Eventually the highest temperature would be lower than for larger pump spot radius. when the pump light power was constant, as the pump spot radius grew larger, the energy density became smaller, and the center maximum temperature became lower. This was the reason why the heat distribution was as shown in Fig. 7 when the depth of focus was zero. However, as the depth of focus increased, the beam of the pump light near the end face gradually increased, which made the temperature distribution more uniform and the distribution area larger, so that the heat dissipation volume was reduced, and the maximum temperature reduction rate of the crystal center was slowed down. But the increase of the size of the pump beam was beneficial to the reduction of the thermal stress of the crystal. Therefore, it was especially important to balance the pump spot radius and the depth of focus to alleviate the thermal effect. Because of the divergence of the pump light, the loss was large, the pump depth increased and the crystal may not produce gain. In the end the laser output phenomenon would not appear and the analysis we mentioned here needed a further experimental verification.

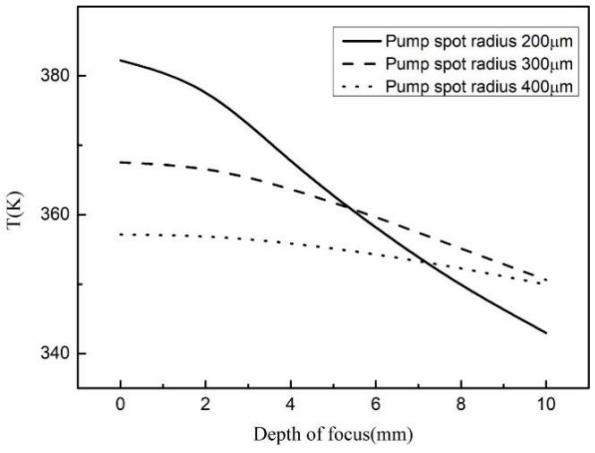

FIG. 7. The variation of the maximum temperature in the crystal as the depth of focus increasing under different spot radiuses.

3.2. Influences of Different Pump Spot Radius and Focusing Depth on Thermal Stress Distribution in Crystals

The stress distributions (a) (b) (c) (d) and the deformation displacements (e) (f) (g) (h) of the crystal at different focusing depths were analyzed when the pump power was 30 W and the radius of the pump spot was 300 μm. The results were shown in Fig. 8.

With the increase of the focusing depth, the maximum stress of the crystal decreased from 32.18 MPa to 28.08 MPa. Although the deformation in Z-axis direction decreased slightly, the reduction was not a larger order of magnitude. Therefore, changing the focusing depth can reduce the thermal distribution, thermal stress and thermal lens effect in the crystal, but the gain of laser crystal was different from different focusing depth, which will affect the laser output power. The numerical simulation provided the theoretical basis for the experiment. In order to obtain a larger laser output, the necessary condition was to slow down the thermal effect, so that the laser crystal can withstand a larger pump power, have a larger conversion efficiency and obtain a higher laser output power.

The stress distributions in the crystal under different pump spot radiuses (i.e. pump spot radius were 200 μm, 300 μm, 400 μm respectively) were analyzed when the pump power was 30 W and the focusing depth was 5 mm. The stress distributions in the crystal are shown in Fig. 9.

With the increased of the focusing coupling ratio, the maximum stress of 30.68 MPa decreased to 27.99 MPa, and the crystal deformation also decreased slightly. According to the alleviation of thermal effect by focusing depth and focusing coupling ratio, changing the focusing coupling ratio and increasing the pump depth can reduce the thermal distribution, thermal stress and thermal lens effect in crystals. Therefore, the thermal lens effect can be mitigated as much as possible to increase the laser output power when the focus depth and the pump depth were reasonably weighed to make the pump depth ratio larger.

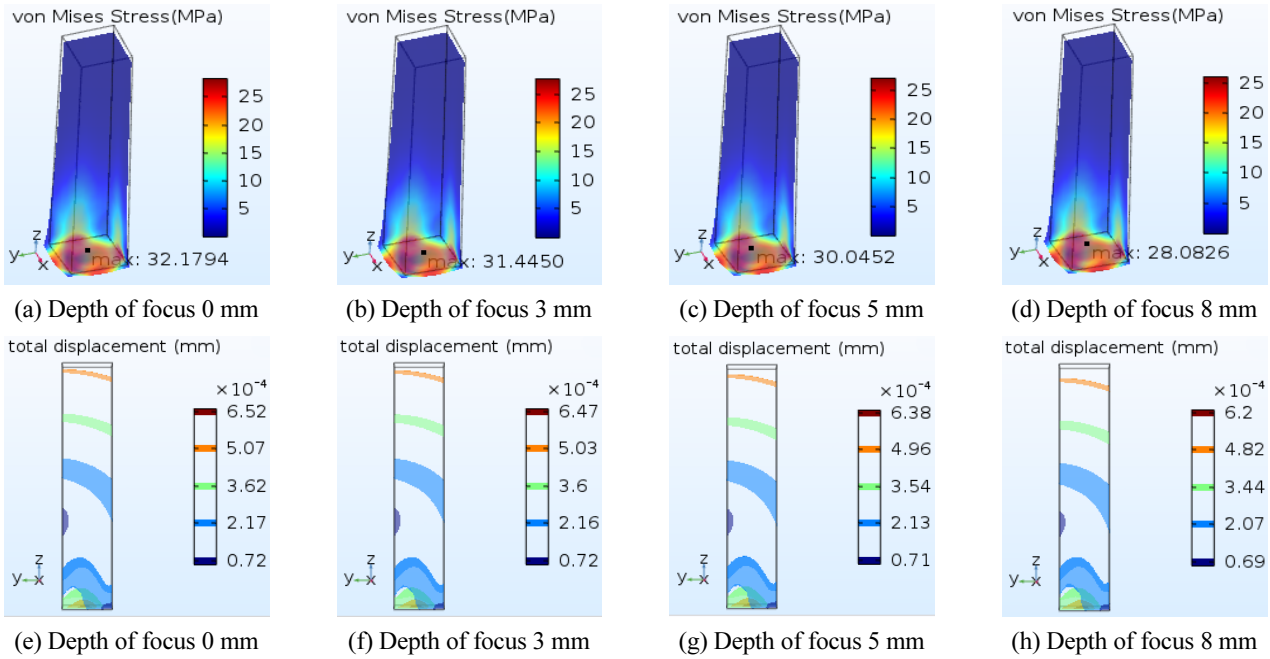

(a) Depth of focus 0 mm (b) Depth of focus 3 mm (c) Depth of focus 5 mm (d) Depth of focus 8 mm

(e) Depth of focus 0 mm (f) Depth of focus 3 mm (g) Depth of focus 5 mm (h) Depth of focus 8 mm

FIG. 8. The stress and deformation in the crystal at different focusing depths when the pumping power was 30 W and the radius of the pumping spot was 300 μm

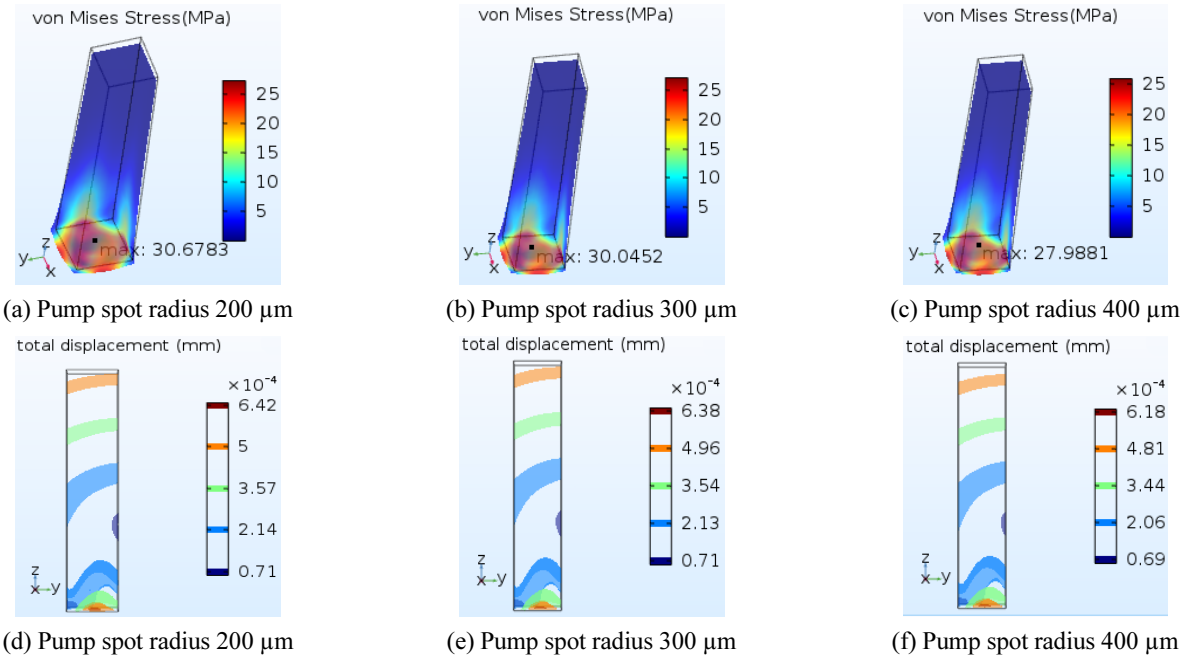

(a) Pump spot radius 200 μm (b) Pump spot radius 300 μm (c) Pump spot radius 400 μm

(d) Pump spot radius 200 μm (e) Pump spot radius 300 μm (f) Pump spot radius 400 μm

FIG. 9. The stress and deformation in the crystal were changed with the radius of the pump spot when the pump power was 30 W and the focusing depth was 5 mm

IV. ANALYSIS OF THE INFLUENCES OF DIFFERENT PUMP SPOT RADIUS AND FOCUSING DEPTH ON OUTPUT POWER

Based on the theoretical analysis, the experimental platform was built to verify the efficiency of the proposed method. By changing the parameters of the focusing coupling mirror and the position of the focusing coupling mirror group from the end of the crystal, the factors such as the output power, slope efficiency and so on were measured and compared to the factors such as the coupling ratio and the focusing depth of optimal power. Figure 10 was a diagram of the experimental device of a single-end-pumped Tm:YAP crystal.

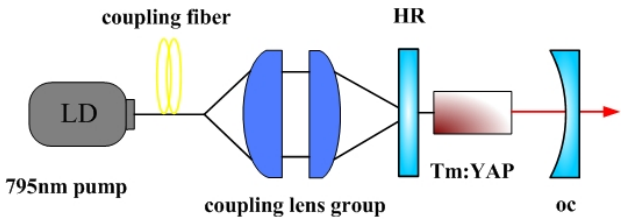

FIG. 10. Diagram of experimental device of LD end-pumped Tm:YAP laser.

The pumping source utilized a semiconductor laser with 795 nm center wavelength, and the maximum output power was 60 W, NA was 0.22. The focusing coupling system was composed of two convex lenses with variable focal length. The surfaces of the lenses were coated with an anti-reflection film of 795 nm. The transmittance of the actual coupled system at 795 nm was more than 95%. The totally reflecting mirror was coated with a film, which had high transmittance ($R < 0.5\%$) at 795 nm and high reflectivity ($R > 99.5\%$) at 1.99 μm; the output mirror was plated with a high transmittance of 10% at 1.99 μm. The Tm:YAP crystal was a domestic crystal with a size of $3 \times 3 \times 15$ mm^3, and both ends of the crystal were plated with a high anti-reflecting film of 795 nm and 1.99 μm ($R < 0.5\%$). The crystal was wrapped with indium foil, which was placed in a copper heat sink, and the entire crystal was cooled by cooling water whose temperature was 289 K. When the pump spot radius corresponding to the focusing coupling ratio of 1 : 1, 1 : 2 and 1 : 3 were 200 μm, 300 μm and 400 μm, the focal lengths of the selected focusing lens group were 50 mm : 50 mm, 50 mm : 75 mm, 25 mm : 50 mm, the focusing depth was 6 mm, we got the output powers shown in Fig. 11.

From Fig. 11, when the focusing coupling ratios were 1 : 1, 1 : 1.5 and 1 : 2, the threshold powers were 11.26 W, 10.08 W and 8.92 W, the maximum output powers were 4.3 W, 6.32 W and 5.66 W, the slope efficiency were 17.98%, 27.44% and 26.18%, respectively. When the coupling ratio is 1 : 1.5 and 1 : 2, the slope efficiency is not much different, but the threshold power of 1 : 2 was lower. The output power of coupling ratio 1 : 1.5 is larger and the output is smoother and more moderate. An experimental study to change the depth of focus coupling with a coupling ratio of 1 : 1.5. is absolutely significant.

By changing the focusing depth of the pump light, the experimental measurement was carried out with the focusing depth of 3 mm, 5 mm, 6 mm and 8 mm, on the premise of ensuring that the laser crystal did not burst and had laser output. The test data are shown in Fig. 12.

When the focusing coupling ratio is 1 : 1.5, the focusing depth are 3 mm, 5 mm, 6 mm and 8 mm, Fig. 12 shows that the threshold powers were 12.46 W, 11.26 W, 10.08 W and 11.26 W, the maximum output powers were 4.51 W, 5.53 W, 6.32 W and 4.46 W, the slope efficiencies were 17.54%, 22.32%, 27.44% and 21.58%, respectively. From the output power, it was easily seen that with the increase of the focusing depth, the power first increased and then decreased, and the slope efficiency also first increased and then decreased. The optimal laser output can be obtained when the focusing coupling ratio of pump light was 1 : 1.5 and the focusing depth was 6 mm. At low power under different focusing depths, the growth trends were much more consistent. With the increase of pump power, the growth trend slowed down. The reason was that with the increase of pump power, the crystal produced a thermal lens effect, while serious thermal lens effect would inhibit laser output. Although laser output can be obtained by pumping laser crystal with pump source, laser output of crystal achieved could be better when the crystal pumped in a specific position. At this time, the thermal effect of pumping light on the crystal was the lowest, which provided theoretical support for obtaining higher laser output power.

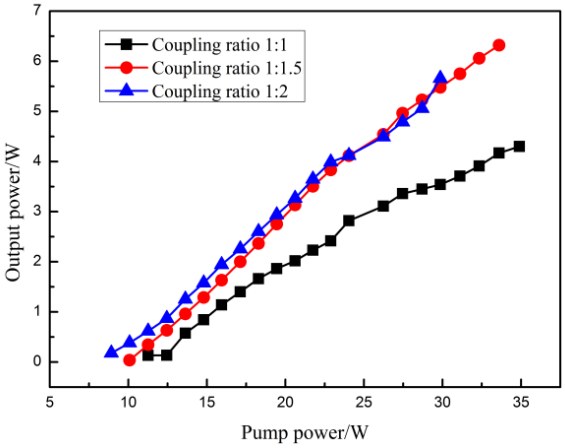

FIG. 11. Output power under different focusing coupling ratios.

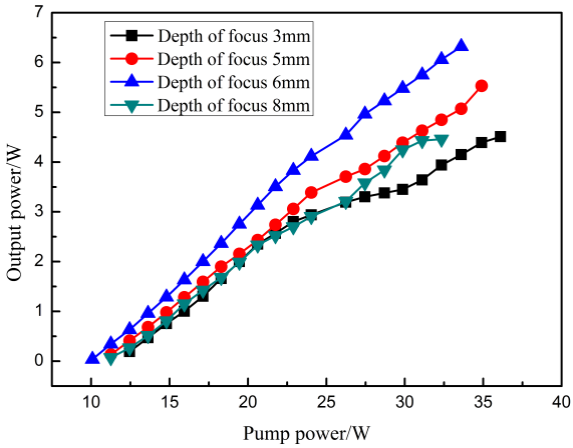

FIG. 12. Output power at different focusing depths.

V. CONCLUSION

High gain of laser crystal was needed when high power laser generated, while the emission cross section of Tm:YAP was small (4.7×10^{-21} cm^2), energy extraction efficiency was low, most of the energy of pump light was concentrated in the crystal and transformed into the heat of the crystal. It was the thermal effect of the crystal that made the crystal unable to withstand large pump light so that it could not produce large gain to obtain high power output. In this paper, COMSOL finite element analysis software was used to simulate the thermal stress of Tm:YAP crystal under different pump focusing depth by coupling solid heat transfer modules and solid mechanics modules. With the increase of pump spot radius, the maximum temperature in the crystal first decreased and then tended to be stable. With the increase of pump focusing depth, the thermal stress decreased in all directions of the crystal. The threshold power was 10.08 W and the maximum output power was 6.32 W when the focus spot radius was 300 μm and the focusing depth was 5 mm. The experimental results were in agreement with the theoretical simulation results. The theory of pump spot radius and focusing depth provided an effective simulation method for alleviating thermal lens effect, which provided theoretical support for the optimization of higher laser output power.

ACKNOWLEDGMENT

This work was supported by the project of Jilin provincial department of education, China (JJKH20181102KJ).

REFERENCES

1. J. Li, S. H. Yang, H. Y. Zhang, D. X. Hu, and C. M. Zhao, "Diode-pumped room temperature single frequency Tm:YAP laser," Laser Phys. Lett. **7**, 203-205 (2010).
2. Q. Yao, Y. Dong, Q. Wang, and G. Jin, "Beam quality improvement by controlling thermal lens spherical aberration in an end-pumped Nd:YVO_4 laser," Appl. Opt. **57**, 2245-2249 (2018).
3. Q. Pengfei, W. Shiyu, G. Zhen, C. Defang, and L. Bingbin, "Adaptive adjusting technique of thermal effect to laser beam quality," Acta Opt. Sin. **37**, 0514001 (2017).
4. K. Yumashev and P. Loiko, "Thermal stress and end-bulging in monoclinic crystals: the case study of double tungstates," Appl. Opt. **56**, 3857-3866 (2017).
5. B. Fang, H. Zhulong, L. Jingliang, C. Xinyu, W. Chunting, and J. Guangyong, "Thermal analysis of double-end-pumped Tm:YLF laser," Laser Phys. **25**, 075003 (2015).
6. P. J. Hardman, W. A. Clarkson, G. J. Friel, and M. Pollnau, "Energy-transfer upconversion and thermal lensing in high-power end-pumped Nd:YLF laser crystals," IEEE J. Quantum Electron. **35**, 647-655 (2017).
7. E. Lippert, H. Fonnum, G. Arisholm, and K. Stenersen, "A 22-watt mid-infrared optical parametric oscillator with V-shaped 3-mirror ring resonator," Opt. Express **18**, 26475-26483 (2010).
8. L. Jingliang, C. Xinyu, Y. Yongji, W. Chunting, B. Fang, and J. Guangyong, "Analytical solution of the thermal effects in a high-power slab Tm:YLF laser with dual-end pumping," Phys. Rev. A **93**, 013854 (2016).
9. G. Chen, "Analytical solutions for temperature and thermal-stress modeling of solid material induced by repetitive pulse laser irradiation," Optik **135**, 16-26 (2017).
10. J. Morris, N. K. Stevenson, H. T. Bookey, A. K. Kar, and A. A. Lagatsky, "1.9 μm waveguide laser fabricated by ultrafast laser inscription in Tm:Lu_2O_3 ceramic," Opt. Express **25**, 14910-14917 (2017).